JOURNAL OF VIROLOGY, June 2011, p. 5651–5663 Vol. 85, No. 11
0022-538X/11/$12.00 doi:10.1128/JVI.01189-10

Identification and Characterization of a Ross River Virus Variant That Grows Persistently in Macrophages, Shows Altered Disease Kinetics in a Mouse Model, and Exhibits Resistance to Type I Interferon▽

Brett A. Lidbury,[1]† Nestor E. Rulli,[1,2,3,4]† Cristina M. Musso,[1]† Susan B. Cossetto,[1] Ali Zaid,[1,2] Andreas Suhrbier,[5] Harald S. Rothenfluh,[6] Michael S. Rolph,[1,3] and Suresh Mahalingam[1,2,3]*

Virus and Inflammation Research Group, Faculty of Applied Science, University of Canberra, Canberra, ACT 2601, Australia[1]; Virus and Inflammation Research Group, School of Biological Sciences, University of Wollongong, Wollongong, NSW 2522, Australia[2]; Emerging Viruses and Inflammation Research Group, Institute for Glycomics, Griffith University, Gold Coast, QLD 4222, Australia[3]; LISIN, Facultad de Ciencias Exactas, Universidad Nacional de La Plata, Buenos Aires, Argentina[4]; Queensland Institute of Medical Research and Griffith University, Brisbane, Australia[5]; and Division of Immunology and Genetics, John Curtin School of Medical Research, Australian National University, Canberra, ACT 0200, Australia[6]

Received 3 June 2010/Accepted 23 February 2011

Alphaviruses, such as chikungunya virus, o'nyong-nyong virus, and Ross River virus (RRV), cause outbreaks of human rheumatic disease worldwide. RRV is a positive-sense single-stranded RNA virus endemic to Australia and Papua New Guinea. In this study, we sought to establish an *in vitro* model of RRV evolution in response to cellular antiviral defense mechanisms. RRV was able to establish persistent infection in activated macrophages, and a small-plaque variant (RRV_{PERS}) was isolated after several weeks of culture. Nucleotide sequence analysis of RRV_{PERS} found several nucleotide differences in the nonstructural protein (nsP) region of the RRV_{PERS} genome. A point mutation was also detected in the E2 gene. Compared to the parent virus (RRV-T48), RRV_{PERS} showed significantly enhanced resistance to beta interferon (IFN-β)-stimulated antiviral activity. RRV_{PERS} infection of RAW 264.7 macrophages induced lower levels of IFN-β expression and production than infection with RRV-T48. RRV_{PERS} was also able to inhibit type I IFN signaling. Mice infected with RRV_{PERS} exhibited significantly enhanced disease severity and mortality compared to mice infected with RRV-T48. These results provide strong evidence that the cellular antiviral response can direct selective pressure for viral sequence evolution that impacts on virus fitness and sensitivity to alpha/beta IFN (IFN-α/β).

Arthritogenic alphaviruses are distributed globally and are maintained in nature by cycles of transmission between hematophagous arthropods (for example, mosquitoes) and enzootic vertebrate hosts (mammals, marsupials, or birds) (33, 53). Nearly all symptomatic infections with these alphaviruses manifest with joint symptoms (arthritis and arthralgia), with myalgia, rash, and lethargy also being common. Ross River virus (RRV) is an Australian alphavirus associated with chronic polyarthritis and causes up to 8,000 cases annually in Australia, with the number of cases reported in new localities increasing (42, 55). During the late 1970s and early 1980s, a number of South Pacific island nations experienced a major outbreak of RRV disease (RRVD) affecting more than 50,000 people (17). More recently, a related virus, chikungunya virus (CHIKV), caused similar rheumatic disease in one-third of the population of Réunion Island in the Western Indian Ocean and an estimated 1.39 million cases in India (22, 23, 37, 52). This outbreak was also associated for the first time with some severe clinical manifestation and mortality (37).

In RRV-infected patients, the disease is usually severe at onset with a gradual resolution over 3 to 6 months (40). Alphavirus-induced rheumatic disease is thought to have a substantial immunopathological component. For example, in animal models tissue damage results from the induction of proinflammatory cytokines and chemokines and recruitment of macrophages in response to infection (29, 43, 55). RRV infects and replicates in human and mouse macrophages, and infection of the mouse macrophage cell line RAW 264.7 results in the establishment of a persistent productive infection (11, 31, 36, 60), which has been regarded as a model of how RRV persists in synovial tissues and produces arthritis/arthralgia (54, 55). Persistence of RRV occurs in RAW 264.7 cells despite the ability of these cells to produce beta interferon (IFN-β) (30, 36), which is known to effectively control alphavirus replication (44).

There is considerable evidence that RRV can persist and establish chronic infection. For example, Soden et al. (50) showed genetic evidence of RRV in synovial tissue of 2 patients from a cohort of 12, 5 weeks after initial symptoms of RRV infection were reported. We have also obtained evidence for chronic infection in a mouse model of RRV infection, with RRV RNA being detected in the ankle joints of mice 3 months after infection (N. Rulli and S. Mahalingam, unpublished data). A number of cell culture models of RRV persistence have also been described. Journeaux et al. (21) established long-term infection (up to 35 days) of primary human synovial cell cultures (which were found to contain "macrophage-like cells"). Small-plaque variants developed in these cultures, suggesting that RRV underwent mutation and adaptation to the

* Corresponding author. Mailing address: Emerging Viruses and Inflammation Research Group, Institute for Glycomics, Griffith University, Gold Coast, QLD 4222, Australia. Phone: 61 7 5552 7178. Fax: 61 7 5552 8098. E-mail: s.mahalingam@griffith.edu.au.
† B.A.L., N.E.R., and C.M.M. are joint first authors.
▽ Published ahead of print on 23 March 2011.

culture conditions. We have previously described persistent RRV infection in macrophages for periods up to 180 days (60). We have also recently observed persistent infection in murine and human osteoblast cultures, suggesting that these cells may also be persistently infected *in vivo* (N. Rulli, R. Li, P. Smith, A. Choo, C. Musso, Y. C. Su, B. Lidbury, and S. Mahalingam, unpublished data). Long-term persistence of antigen from the related alphavirus chikungunya virus has recently been found in perivascular synovial macrophages in one chronically infected patient 18 months after initial infection (19). With a macaque model, Labadie et al. observed long-term chikungunya virus infection in joints, muscles, lymphoid organs, and liver, which may explain the long-lasting disease symptoms observed in humans (26). In addition, the authors identified macrophages as the main cellular reservoirs during the late stages of chikungunya virus infection *in vivo* (26).

Here we describe the generation of a small-plaque mutant of RRV (RRV_{PERS}) derived from persistently infected RAW 264.7 macrophages that had been stimulated with lipopolysaccharide (LPS) to induce an antiviral phenotype, including the production of alpha/beta interferon (IFN-α/β) (30, 34). RRV_{PERS} displayed significantly increased resistance to IFN-β-induced antiviral activity compared to the parental RRV-T48 virus. RRV_{PERS} also induced lower levels of type I IFN than RRV-T48 and was able to inhibit type I IFN signaling. RRV_{PERS} infection of mice resulted in increased morbidity, mortality, and disease kinetics. Sequencing of RRV_{PERS} identified 12 substitutions in the E2 and nsP regions of the RRV_{PERS} genome. The study provides the evidence for an arthrogenic alphavirus that specifically targets host IFN-α/β responses, leading to increased pathogenicity. RRV_{PERS} appears to have evolved specific strategies to counteract the IFN-α/β-induced antiviral responses, and we speculate that a similar evolution may occur *in vivo*.

MATERIALS AND METHODS

Ross River virus and macrophage cell line. Ross River virus (RRV) derived from an infectious clone of strain T48 (originally designated RR64) (25) was used to initially infect the mouse macrophage cell line RAW 264.7 (ATCC TIB-71) cultured at 5.0×10^5 cells per well/ml in 24-well trays (Nunc, Roskilde, Denmark). To produce infectious virus, pRR64 was linearized by SacI digestion and transcribed *in vitro* from the cDNA using SP6 RNA polymerase, and the infectious RNA was transfected into BHK-21 cells as previously described (25). Viral stocks were propagated in Vero cells (ATCC CCL-81), as previously described (28), and no virus stock exceeded two Vero cell passages prior to experimental use. Viral titers were determined by plaque assay with Vero cells (see details below).

RAW 264.7 cells were maintained in Eagle minimal essential medium (EMEM) (Thermo-Trace, Melbourne, Australia) supplemented with 5% heat-inactivated fetal calf serum (HI-FCS) (Thermo-Trace), 1% penicillin-streptomycin, 1 to 1.5% sodium bicarbonate, and 2.0 mM L-glutamine (Thermo-Trace). Following RRV infection, 5.0 ng/ml lipopolysaccharide (LPS) (*Escherichia coli* serotype 0111:B4; Sigma) was added to the cultures, and this LPS concentration was maintained over the entire experimental period.

RAW 264.7 cells were infected with RRV at a multiplicity of infection (MOI) of 0.1 (in PBS plus 1% HI-FCS) for 1 h at 37°C. The virus inoculum was removed, and 1.0 ml of fresh EMEM-FCS was added to each well, after which the infected cultures were further incubated at 37°C (5.0% CO_2, 95% humidity). Culture supernatants were collected at several time points (days 1, 2, 5, 14, and 21) for RRV plaque assay. Fresh and warmed EMEM-FCS (500 μl per well) was added to each well after sample collection.

Detection and purification of small-plaque RRV. The parent RRV-T48 plaques are visible on Vero cell monolayers by day 2 postinfection. To visualize the small plaques by eye, an extra day of incubation was required at room temperature. At day 14 postinfection (approximately 90% small plaques), small plaques were purified by picking individual isolated small plaques from the stained Vero cell monolayer. An isolated large plaque was also purified from the same culture. Infected Vero monolayers were incubated under a semisolid agar overlay (complete M199 [Thermo-TRACE] or DMEM supplemented with 2.0% FCS, 0.02% DEAE-Dextran, 4.0% heat-inactivated newborn serum [Thermo-TRACE], and 1.0% agar [Bacto Laboratories Pty. Ltd., Liverpool, Australia], penicillin-streptomycin, L-glutamine, and sodium bicarbonate at the final concentrations described above), and at day 2 or 3 of incubation, 0.02% neutral red in phosphate-buffered saline (PBS) (pH 7.4) supplemented with 2.0% penicillin-streptomycin and 0.7% agar was added to the agar overlay and the plaque assays were incubated for a further 1 to 2 h at 37°C. The agar plugs were carefully removed, and individual plaques were picked by holding a pipette tip directly on top of the plaque and gently pipetting 10 μl of complete EMEM-FCS five times onto the plaque. After the final wash, the 10-μl sample was diluted in 1.0 ml of complete EMEM-FCS and added to a fresh monolayer of confluent Vero cells in a 25-cm^3 flask (Corning, NY), and the culture was incubated at 37°C (5.0% CO_2, 95% humidity). As soon as cytopathic effect was observed in the Vero cell monolayer (2 to 3 days postinfection), the infectious supernatants were collected and centrifuged to remove cell debris ($400 \times g$). Plaque assays were carried out to confirm the small-plaque phenotype in fresh Vero cell cultures and to estimate the virus concentration ($\log_{10}$ PFU/ml). This plaque purification procedure was then repeated with isolated plaques found on the fresh Vero cell monolayers. After the second round of purification, stocks of small- and large-plaque (parent) virus were grown in fresh Vero cell cultures, as described above; these stocks were used for all subsequent experiments and nucleotide sequence analyses. The small-plaque RRV was designated RRV_{PERS}. These studies are covered by a license from the Australian Government's Office of Gene Technology Regulator (license number DNIR 389/2006).

RRV neutralization by polyclonal anti-RRV sera and anti-RRV-E2 monoclonal antibodies. Murine anti-RRV polyclonal serum was added to Hanks balanced salt solution (HBSS) (pH 7.2), Thermo-Trace, Melbourne, Australia) containing 2% (wt/vol) bovine serum albumin (BSA) (Sigma, Missouri) to a final dilution of 5.0×10^{-1}. Serial 10-fold dilutions of this polyclonal serum were then prepared. An equal volume of HBSS-BSA containing 200 PFU of RRV-T48 or RRV_{PERS} was added to the diluted antibody. The antibody-virus preparations were incubated at 37°C for 1 h, after which 100 μl was plated on confluent Vero cell monolayers and incubated at 37°C (5% CO_2, 95% humidity) for 48 h. The monolayers were stained for plaque enumeration exactly as described above.

Reaction of RRV_{PERS} or RRV-T48 with E2-specific monoclonal antibodies (MAbs) was performed exactly as described above for polyclonal sera. MAbs designated 10C9, 3C4, and E7 were generously provided by Ron Weir (Australian National University) and Roy Hall (University of Queensland) from a previously described antibody panel (6).

RNA extraction and isolation of RRV genomic cDNA by Reverse transcriptase (RT) PCR. Vero cells cultured in 25-cm^3 flasks were infected with of RRV_{PERS} at an MOI of 0.1. As soon as cytopathic effect was observed (36 h postinfection), culture medium was removed and cells were treated with 200 μl of acidified (pH 4.5) guanidinium isothiocyanate-phenol-sodium acetate (buffer), following the protocol of Chomczynski and Sacchi (7). To isolate RRV-specific RNA from the total RNA collected, reverse transcription (SuperScript preamplification system for first-strand cDNA synthesis; Invitrogen, Carlsbad, CA) was performed using either the RRV E2-specific antisense primer P2 or P5 (Table 1). Standard PCR was then carried out with the same antisense primer as used for reverse transcription and primer P1 (sense primer; see Table 1). *Taq* DNA polymerase, deoxyribose nucleoside triphosphates (dNTPs), buffers, and magnesium chloride ($MgCl_2$) were supplied by Qiagen (*Taq* PCR core kit, catalog no. 201223) (Hilden, Germany), and RRV E2 primers were synthesized by GeneWorks (Adelaide, South Australia).

To specifically amplify the entire RRV E2 cDNA, the following cycling and temperature protocol was used: denaturation at 94°C for 2 min (1 cycle), followed by sequential denaturation, primer annealing, and strand elongation by *Taq* cycles of 94°C (30 s) plus 60°C (40 s) plus 72°C (50 s) (35 cycles) and 72°C (5 min) (1 cycle). For the primer sets used to amplify the entire RRV E2 gene (primers P1 plus P2 or P1 plus P5) (Table 1), this protocol was performed with equal efficiency.

Amplification of RRV nsP1 to nsP4 was achieved after the extraction of total RNA from infected Vero cells, as described above, followed by RT using oligo(dT) or gene-specific primer (Table 2) and the Superscript first-Strand synthesis system (Invitrogen) to produce a single-stranded cDNA of the RRV nsP sequence. The PCR amplification of nsP fragments utilized Proof Start DNA polymerase (Qiagen), and reaction conditions were as recommended by the manufacturers. Samples were amplified through 45 cycles of primer annealing for

TABLE 1. Primers used for RT-PCR isolation and nucleotide sequence analysis of the RRV E2 gene from a small-plaque variant of RRV-T48

Primer	Polarity	Position (5′)[a]	Oligonucleotide sequence (5′–3′)[b]	Product size (bp)
P1	+	8545	GAAACAGATCACGCCACCGC	1,289
P2	−	9834	CTGCGTTCGCCCTCGGTGCG	
P3	+	8946	GTCCAATACAAGCACGACCC	
P4	−	9454	TAGGAGAAGAGCGTCGGATG	
P5	−	10035	GAATTGTGGCTGTGTGCTCG[b]	1,490 (with P1)

[a] Position of primer in complete RRV genome (refer to reference 10).
[b] Primers used for RT-PCR amplification of RRV E2. The E2 gene is 1,268 bp in length (position 8566 to 9834) and is situated between the E3 and 6K coding regions of the RRV genome (10).

1 min at 58°C, elongation for 1 min at 72°C, and denaturation for 1 min at 94°C. The primers used for reverse transcription and subsequent cDNA amplification of viral nsP (Table 2) were designed on the basis of the complete genomic sequence of RRV strain 48 (T48) (10). Prior to sequencing, the quality of the PCR products were checked by agarose gel electrophoresis and ethidium bromide staining.

Nucleotide sequencing of the RRV_{PERS} E2 and nsP genes. ABI Prism BigDye Terminator cycle sequencing chemistries (PE Applied Biosystems, California) were used to generate the specific RRV E2 and RRV nsP sequences prior to gel analysis, as described below. Thermal cycling protocols and conditions were run according to the manufacturer's recommendations.

RRV E2 gene sequencing. Template cDNA was included in the sequencing reaction at 0.5 μg per reaction. The entire RRV-E2 cDNA sequence was obtained using the primers listed in Table 1. Further confirmation of the single base change found for RRV_{PERS} was demonstrated by m13 sequencing of the RRV-E2 cDNA after cloning into pUC-19. Briefly, the entire RRV-E2 cDNA was cloned into the EcoRI site of pUC-19 at a 3:1 insert-to-vector ratio with T4 DNA ligase (Promega Corp.). To facilitate cloning, the ends of the RRV-E2 cDNA were modified during PCR amplification to incorporate EcoRI sites; this was achieved by the addition of GCGCGAATTC to the 5′ end of primers P1 and P2 (Table 1) (45). Amplification and sequencing were repeated to confirm base changes. After the above preparations, gel analysis of the RRV-E2 gene sequence was performed through the DNA Sequencing Analysis Facility at the University of New South Wales, Sydney, Australia.

nsP gene sequencing. PCR products were cut from the 1% agarose gel and purified using a minicolumn system (Millipore). PCR sense and antisense primers (Table 2) were used as sequencing primers to ensure full coverage of the RRV nsP1 to nsP4 genes. Amplification and sequencing were repeated to confirm base changes. Thermal cycle sequencing reactions and gel analyses were carried out at the Australian National University (ANU) Sequencing Core Facility.

Growth kinetics of RRV. Vero, HEp-2 (a human laryngeal epithelial cell line), and RAW 264.7 cells were cultured in EMEM-FCS at 37°C (5.0% CO_2, 95% humidity). Cells were infected with RRV-T48 or RRV_{PERS} at an MOI of 0.1. Culture supernatants were collected at 12, 24, and 48 h postinfection, and viral growth was assessed by plaque assay on Vero cell monolayers.

In a separate experiment, RAW 264.7 cells were pretreated with medium containing anti-murine IFN-α and anti-murine IFN-β (10^4 U/ml; both from R&D Systems) for 1 h at 37°C. The treated cells were then infected with RRV-T48 or RRV_{PERS} at an MOI of 0.1 for 1 h at 37°C. Cells were then washed, and fresh medium containing 10^4 U/ml of anti-murine IFN-α and anti-murine IFN-β antibodies was added to the cells. Supernatants were collected at 12, 24, and 48 h postinfection, and viral growth was assessed by plaque assay on Vero cell monolayers.

Determination of RRV infectivity by IFA. The percentage of infected cells was determined by immunofluorescence assays (IFA) at 6, 12, and 24 h postinfection as described previously (30). Briefly, confluent virus-infected and noninfected control cells in glass chamber slides were fixed for 1 min with a 1:1 ratio of

TABLE 2. Primers used for nucleotide sequence analysis of the RRV nsP1 to nsP4 genes from RRV_{PERS}

Primer	Polarity	Position (5′)	Oligonucleotide sequence (5′–3′)	Product size (bp)
P1	+	7	GGACGTGTGACATCACCGTTC	655
P2	−	662	GGAATACGTTGGGTATGCGCC	
P3	+	603	GGATTCGACACCACCCCATTC	650
P4	−	1253	CTTGCTGAAAGCTTGGGCCAC	
P5	+	1147	TACTGGTGGGGTTGAACCAAC	697
P6	−	1844	TCCTGAGTGCGTCATGATTGTC	
P7	+	1744	CGCGTACCTGATCTTGTCTC	708
P8	−	2452	TGACAGGCAAATGCTTCGTCC	
P9	+	2352	AGAGGACTGGATGTAACAGCC	630
P10	−	2982	ACACCTTTATCCACGGGTCTC	
P11	+	2939	GCTGGTGTGGAAAACACTGTC	641
P12	−	3580	TGGTATCCGGGAAGCTTCTTC	
P13	+	3361	GCGAAGTCGCCCGTAAGTTTG	776
P14	−	4137	CATTGACAACCGCCTCTTCGG	
P15	+	4076	ACCCTCATACCGTGTGCGTAG	756
P16	−	4832	CGAATCGGCGTCCTCAACAG	
P17	+	4795	GCATCAGAACGAAATGCCCTG	777
P18	−	5572	TCAACCGGCTCGCGCATTTTG	
P19	+	5514	CTGAAGATCTGGAGGTACTCAC	827
P20	−	6341	TAGAGTGGGTAGCTCTCTCATC	
P21	+	6242	CGCGGTCCCATCACCATTTC	677
P22	−	6919	ATTTCCCCGAACGCTGCCTC	
P23	+	6840	TTGACGGCACTGATGCTGTTG	680
P24	−	7520	TTTAGGACCGCCGTAGAGGTG	
P25	+	7311	CAAGATGAAGATCGTAGGCGTG	439
P26	−	7750	CTGTTTGGTGGTTAGTGCAGAG	

acetone-methanol, followed by overnight incubation at 4°C in PBS. The cells were then incubated at 37°C for 2 h with mouse anti-RRV hyperimmune ascitic fluid diluted (10^{-3}) in PBS containing 1% HI-FCS, followed by three washes with sterile PBS. This was followed by incubation of the cells with fluorescein isothiocyanate (FITC)-conjugated sheep anti-mouse IgG antibody (Silenius, Melbourne, Australia) in PBS (1% HI-FCS) for 1 h at 37°C. Cells were then washed three times with sterile PBS. Cells were counted with a Leica fluorescence microscope.

IFN-β treatment of RAW 264.7 cells. RAW 264.7 cells were cultured in EMEM-FCS containing 10, 50, or 100 IU/ml of recombinant mouse IFN-β (catalog no. PMC4024; Invitrogen, Australia) for 24 h prior to infection with 0.1 MOI of parent RRV-T48 or RRV_{PERS}. Supernatants were collected 12 h postinfection (p.i.) and titrated by plaque assay on Vero cell monolayers for determination of virus titers.

Plasmids and DNA transfection for luciferase assay. The luciferase reporter plasmid constructs pIFN-β (−125/+72) Lucter and pISRE (9-27) Lucter were used in experiments involving transfection of RAW 264.7 cells and Vero cells, respectively. Plasmid DNA was transfected using the GeneJammer transfection reagent, following the manufacturer's protocol (Stratagene). For RAW 264.7 cell experiments, cells were transfected with 2 μg of pIFN-β (−125/+72) Lucter together with an equal amount of pCMV-βGal plasmid (Promega) as an internal control. Cells were cultured for a further 24 h and then were infected with 0.1 MOI of RRV-T48 or RRV_{PERS}. Cells were harvested at 12 h postinfection and processed for measurement of luciferase activity (luciferase reporter assay kit; Promega) and β-galactosidase activity (β-galactosidase reporter assay kit; Promega) according to the manufacturer's instructions. Luciferase activity was read on an Ascent Luminoskan luminometer (Pathtech), and β-galactosidase activity was measured on a UV-visible microplate reader at 495 nm (Bio-Rad). For Vero cell experiments, cells were transfected with 2 μg of pISRE (9-27) Lucter and 2 μg pCMV-βGal (Promega). Cells were then infected with RRV-T48 or RRV_{PERS} at an MOI of 5. Twelve hours later, IFN-β (100 IU/ml) was added to cell culture and luciferase expression was measured at 6 h following incubation.

Quantitative real-time PCR. Total RNA was isolated from RAW 264.7 cells infected with RRV-T48 or RRV_{PERS} at an MOI of 0.1 using TRIzol (Invitrogen Life Technologies). Real-time PCR for IFN-β was carried out on the Rotor-Gene RG-3000 thermal cycler (Corbett-Research, Australia), using Quantitect primer assay kits (Qiagen, Germany) based on quantification of the SYBR green I fluorescent dye. Data were normalized to data for glyceraldehyde-3-phosphate dehydrogenase (GAPDH).

For viral quantitation by real-time PCR, the method of Shabman et al. was used (48). Briefly, RNA was purified from infected culture medium using a MagMAX viral RNA isolation kit (catalog no. AM1939; Ambion). Virion RNA was reverse transcribed using leukemia virus reverse transcriptase (invitrogen), and the cDNA was used for quantitative real-time PCR. TaqMan primers/probes specific for the NSP3 region of RRV were used as described previously (48). A DNA standard curve for the RRV genome was generated to ensure optimal primer-probe efficiency and assign relative genome numbers for sample comparison.

Semiquantitative RT-PCR analysis of the RRV E2 gene. Total RNA was extracted from RAW 264.7 cells infected with RRV-T48 or RRV_{PERS} at an MOI of 0.1 using TRIzol (Invitrogen Life Technologies). Primer and probe sequences for RRV E2 and hypoxanthine phosphoribosyltransferase (HPRT) have been described (34, 60). The cycle numbers used for amplification of each gene product are in the linear phase of amplification: E2, 25 cycles; hypoxanthine phosphoribosyltransferase (HPRT), 23 cycles. The amplified DNA was analyzed by gel electrophoresis and Southern blotting and detected using the ECL detection system as recommended by the manufacturer (Amersham). PCR amplification with the HPRT reference gene was performed to assess variations in cDNA or total RNA loading between samples. Relative transcript levels were quantified in arbitrary units using the ImageJ software program (image processing and analysis in Java; http://rsb.info.nih.gov/ij/).

IFN-β ELISA. The concentration of IFN-β in samples was determined by enzyme-linked immunosorbent assay (ELISA) (Biomedical Laboratories) according to the manufacturer's instructions.

Western blot analysis. Total protein was obtained from RAW 264.7 cells stimulated with 50 IU/ml IFN-β 24 h prior to RRV infection (MOI = 0.1), and cell lysates were analyzed by 10% sodium dodecyl sulfate-polyacrylamide gel electrophoresis and Western blotting performed using a polyclonal antibody against the RRV E2 glycoprotein (kindly provided by L. Hueston, Westmead Hospital, Sydney, Australia). Fluorescence was detected by ECL Plus immunofluorescence (Amersham). In a separate experiment, HEp-2 cells were infected for 12 hwith parent RRV-T48 or RRV_{PERS} at an MOI of 5, followed by IFN-β treatment (100 IU/ml) for 30 min or no treatment. Proteins were analyzed from whole-cell protein extracts by immunoblotting as previously described (49). The following primary antibodies recognizing nonphosphorylated and phosphorylated (P) forms of STAT-1 and STAT-2, α-actin (loading control), and secondary antibody were purchased from the indicated manufacturers: anti-STAT-1 (sc-345), anti-P-STAT-1 (sc-135648), anti-STAT-2 (sc-476), anti-P-STAT-2 (sc-21689), and anti-α-actin (from Santa Cruz Biotechnology) and peroxidase-conjugated goat anti-rabbit antibody (from Jackson Immunoresearch).

Outbred mouse mortality and morbidity studies. Mice were obtained from the Animal Resources Centre, Canning Vale, Western Australia. Fourteen-day-old Swiss outbred mice were inoculated intraperitoneally (i.p.) with 100 μl PBS–1% FCS containing various doses (from 10^4 to 10^6 PFU) of plaque-purified parent RRV (RRV-T48) or purified RRV_{PERS}. Plaque assays on T48 and RRV_{PERS} stocks used in mouse experiments were performed in parallel using the same batch of Vero cells. Both parent RRV and RRV_{PERS} showed stock titers of $>10^8$ PFU/ml. In addition, to reflect equal particle doses, specific infectivity of the RNA of each virus was determined by the overlay of agarose on transfected BHK-21 cells and the enumeration of plaques from each virus. The specific infectivities of RRV-T48 and RRV_{PERS} were found to be similar (for RRV-T48, 1.8×10^5 PFU per μg of RNA; for RRV_{PERS}, 1.9×10^5 PFU per μg of RNA). Experiments were performed to compare RRV_{PERS} and parent RRV titers in mouse serum at 24 h p.i. with 10^4 PFU RRV. Control mice inoculated i.p. with PBS alone showed no mortality or disease symptoms over the experimental period. All experiments were approved by the Animal Ethics Committee of the University of Canberra and Australian National University. In a separate experiment, 5-week-old Swiss outbred mice were inoculated in the right hind-leg footpad with 10^4 PFU RRV_{PERS} or RRV-T48. At 1 day postinfection, mice were sacrificed and popliteal lymph nodes were collected and homogenized for IFN-β ELISA analysis.

Outbred mouse RRVD studies. The experimental approach used for murine RRV infection and monitoring of clinical disease was as described previously by Lidbury et al. (28, 29). Eighteen-day-old mice were inoculated subcutaneously in the pectoral area with 10^4 PFU of RRV diluted in PBS (pH 7.2) in a 20-μl volume. Mock-inoculated animals were injected with the diluent alone. Mice were scored for disease symptoms every 24 h. Signs of disease were determined by assessing grip strength and altered gait. Mice were scored as follows: 0, no disease; 1, ruffled fur; 2, very mild hind limb weakness; 3, mild hind limb weakness; 4, moderate hind limb weakness; 5, severe hind limb weakness/dragging; 6, complete loss of hind limb function; 7, moribund; 8, dead. The experiments were approved by the Animal Ethics Committee of the University of Wollongong.

Statistical analysis. The significance of differences between experimental groups was analyzed by one-way analysis of variance (ANOVA) followed by Bonferroni's test. Values were reported as the means ± standard errors (SEM). For disease scores, data were analyzed by using the Mann-Whitney test. For survival studies, survival curves were analyzed by using the log rank test. Statistical analyses were performed using the GraphPad 63721 Prism software program, version 4.0b (GraphPad Software Inc.). Differences in means were considered significant at P values of <0.05.

RESULTS

Kinetics of small-plaque RRV growth. To study the interplay between virus and host antiviral pathways, we established persistent RRV infection in macrophages that had been treated with LPS to stimulate antiviral activity. In LPS-treated RAW 264.7 cell cultures, small plaque mutants of RRV first emerged at day 5 postinfection and coexisted with large (parent RRV) plaques. By day 14 postinfection, 90% of plaques visible on Vero cell monolayers were of the small phenotype (Table 3). In cultures treated with polymyxin B sulfate (to remove LPS) at the same time as RRV infection, the appearance of small plaques was delayed until day 14 postinfection (data not shown). RRV_{PERS} maintained a small-plaque phenotype after several rounds of plaque purification and growth in fresh Vero cell cultures (Fig. 1A).

To determine whether there were differences in the growth of RRV-T48 and RRV_{PERS}, kinetics of virus growth were

TABLE 3. Mean RRV titers in RAW 264.7 murine macrophages over 21 days p.i.[a]

Day p.i.	Mean RRV titer (log_{10} PFU/ml) ± SEM
1	4.77 ± 0.02 (0 small plaques)
2	5.27 ± 0.16 (0 small plaques)
5	5.34 ± 0.11 (27, 5.8, 8.5[b])
14	5.93 ± 0.14 (89, 93, 91[b])
21	4.01 (80[b,c])

[a] Cells were infected at an MOI of 0.1 on day 0 ($n = 3$) and cultured with 5 ng/ml LPS. Virus used in this experiment was derived from the RRV-T48 genetic clone (RR64).

[b] Proportion(s) (%) of small RRV plaques observed on Vero cell monolayers after RAW 264.7 macrophage infection ($n = 3$ except where otherwise noted) over a 21-day period. Parent virus (RRV-T48) presents as a "large" plaque on Vero cell monolayers (Fig. 1). At days 1 and 2 post-RRV-T48 infection, only large plaques were observed.

[c] $n = 1$.

compared in Vero, HEp-2, and RAW 264.7 cells. There were no significant differences in growth kinetics observed in Vero cells (Fig. 1B) (which do not make IFN-α/β) and in HEp-2 cells (Fig. 1C). In contrast, in RAW 264.7 cells, growth kinetics for RRV-T48 and RRV_{PERS} differed, with RRV_{PERS} producing >1 log_{10} more virus at 24 and 48 h postinfection (Fig. 1D). Importantly, growth kinetics for RRV-T48 and RRV_{PERS} were not significantly different in RAW 264.7 cells pretreated with anti-murine IFN-α and anti-murine IFN-β antibodies (Fig. 1E). These findings suggest that the enhanced growth of RRV_{PERS} in RAW 264.7 cells involves modulation of the IFN-α/β response.

Characterization of RRV_{PERS} using monoclonal antibodies. Using polyclonal anti-RRV antibodies, plaque inhibition assays (PIA) showed a 50% neutralization endpoint for small-plaque RRV identical to that for the parent RRV-T48 virus (1.9×10^{-5} versus 1.5×10^{-5}), confirming the identity of the small-plaque virus as RRV (Table 4).

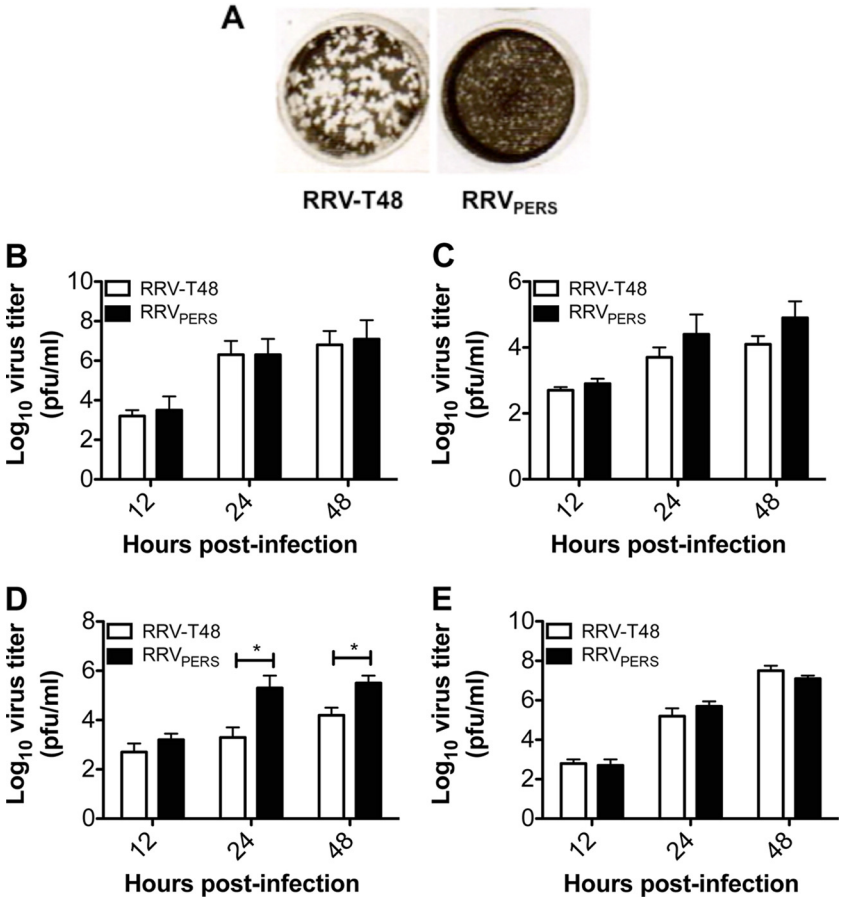

FIG. 1. Differential plaque morphology and growth kinetics of RRV_{PERS} compared to those of RRV-T48. (A) Plaque morphology on Vero cell monolayers for parent Ross River virus strain T48 (RRV-T48) and RRV_{PERS}. Both RRV-T48 and RRV_{PERS} plaques were purified from the supernatants of RRV-T48-infected RAW 264.7 cultures at day 14 postinfection, and new viral stocks were regrown in fresh Vero cell cultures, after which plaque morphology was confirmed by plaque assay. (B and D) Growth kinetics of RRV-T48 and RRV_{PERS} in Vero (B), HEp-2 (C), or RAW 264.7 (D) cells infected at an MOI of 0.1. (E) RAW 264.7 cells were pretreated with 10^4 U/ml of anti-murine IFN-α and anti-murine IFN-β antibodies (R&D Systems) for 1 h at 37°C. The cells were then infected with 0.1 MOI RRV-T48 or RRV_{PERS} for 1 h at 37°C. The virus inoculum was discarded, and cells were rinsed with medium. Fresh medium containing 10^4 U/ml of anti-murine IFN-α and anti-murine IFN-β antibodies was added to the monolayer for an additional 48 h at 37°C. Culture supernatants were collected at various time points post-RRV infection, and viral growth was assessed by plaque assay on Vero cell monolayers. The assay limit of detection is 2.0 log_{10} PFU/ml. Significant differences in virus titers ($P < 0.05$) are marked with an asterisk.

TABLE 4. Antibody-mediated inhibition of RRV plaque formation on Vero cell monolayers by anti-RRV polyclonal sera or RRV E2 protein-specific monoclonal antibodies[a]

Anti-RRV antibody	Highest antibody dilution to achieve 50% RRV plaque inhibition	
	RRV-T48	RRV_{PERS}
Polyclonal anti-RRV[b]	1.5×10^{-5}	1.9×10^{-5}
MAb E7[c]	7.5×10^{-5}	$<10^{-1}$
MAb 10C9[c]	1.2×10^{-4}	3.5×10^{-4}
MAb 3C4[c]	1.2×10^{-6}	$<10^{-1}$

[a] All antibodies were titrated by 1/10 serial dilution from $1/50 \times 10^6$ to $1/5 \times 10^6$ prior to mixing with 200 PFU of purified RRV.
[b] Polyclonal antibody to RRV raised in ascitic fluid to PEG-purified RRV-T48.
[c] Specific for the E2 protein of RRV.

TABLE 5. Predicted amino acid differences in the nsP1 to nsP4 and E2 proteins of persistent RRV_{PERS} compared to sequence of the parent, RRV-T48[a]

Protein	Amino acid position	Amino acid (nucleotides)		Conservation (+/−)	Nucleotide position
		RRV-T48	RRV_{PERS}		
nsP1	143	R (AGA)	T (ACA)	−	450
	147	A (GCT)	S (TCT)	−	461
	154	X (NGG)	A (GCG)	+/−	483
	303	R (GCC)	P (CCC)	−	929
	499	K (AAG)	N (AAT)	−	1519
nsP2	239	L (TTG)	F (TTT)	+	2341
	240	N (AAC)	D (GAC)	−	2342
	306	Y (TAC)	H (CAC)	−	2540
	634	H (CAT)	Q (CAA)	−	3526
nsP3	337	S (AGC)	I (ATC)	−	5028
nsP4	563	K (AAG)	N (AAC)	−	7321
E2	116	E (GAG)	V (GTG)	−	8913

[a] Based on nucleotide sequence analysis of the nsP1 to -4 region and E2, 6K, and E1 (structural) regions of the RRV genome. (Silent mutations are not included). Amino acid residues are numbered from the N terminus of each nsP and E2 protein. The single-letter amino acid code is used. Conservative amino acid differences are indicated by "+." Amino acids that could not be deduced due to nucleotide ambiguity (N) are shown as an X. Nucleotides are numbered from the 5′ terminus of the RRV Sp sequence. The GenBank accession number for RRV E2 cDNA is M20162.

PIA analysis using three monoclonal antibodies (MAbs) specific to the viral E2 protein revealed differences in neutralization. For two of the three MAbs tested (E7 and 3C4), 50% plaque neutralization antibody titers were significantly lower for RRV_{PERS} than for the parent RRV-T48 virus (Table 4). The relative resistance of RRV_{PERS} to neutralization by MAbs E7 and 3C4 suggested an alteration in the RRV-E2 sequence in the small-plaque variant.

Nucleotide sequence *of* RRV_{PERS}. The E2 gene in RRV_{PERS} and RRV-T48 E2 were sequenced using RRV E2-specific primers (Table 1) that covered the entire 1,266-bp sequence. E2 PCR products were also cloned into the EcoRI site of pUC-19, and forward and reverse m13 nucleotide sequencing was performed. Analysis of the E2 sequences revealed a single nucleotide change at position 347 (5′→3′) of the RRV E2 gene sequence (RRV-T48, [GAG]; small-plaque RRV, [GUG]). This genetic alteration resulted in a nonconservative change from the acidic (negatively charged) glutamic acid residue at amino acid position 116 of the parent virus E2 protein to a nonpolar hydrophobic valine residue in RRV_{PERS} (Table 5). Sequence analysis of the untranscribed regions (UTRs) and other genes encoding RRV structural proteins outside the E2 gene (e.g., 6K, E1, and E3) did not show any differences between RRV_{PERS} and RRV-T48 (data not shown).

The complete nsP region of RRV_{PERS} was sequenced and compared with sequence of the parent strain virus, RRV-T48 (NCBI accession number DQ226993). Sequence analysis was started from 21 nucleotides 5′ of the polyprotein start codon (AUG) (position 59 in full-length RRV sequence) and finished at the nsP4 stop codon (UAA; position 7523). The genomic organization was the same for RRV_{PERS} and RRV-T48. Four silent mutations and 11 mutations resulting in single amino acid substitutions were identified in RRV_{PERS} nsP1 to nsP4 (Table 5). No base deletion or nonsense mutations were found.

RRV-T48 and RRV_{PERS} nsPs thus showed an average amino acid identity of 99%. Eighty-three percent (83%) of the amino acid substitutions are within the nsP1 and nsP2 regions. The majority of amino acid changes were nonconservative. Interestingly, a nonconservative change of arginine (basic) to proline (hydrophobic) was present near the center of the nsP1 protein (Pro-303), a region that is highly conserved among alphaviruses (10).

RRV_{PERS} induces less IFN-β mRNA expression and protein production. To determine whether RRV-T48 and RRV_{PERS} differentially affect IFN-β production, the levels of IFN-β mRNA were measured in RAW 264.7 cells infected with each virus. The increase in IFN-β mRNA expression in response to RRV_{PERS} infection was significantly less than that in cells infected with RRV-T48 (Fig. 2A). This reduction in IFN-β mRNA expression occurred despite the fact that RRV_{PERS}-infected cells contained about 4-fold more genomic RNA than RRV-T48-infected cells as determined by semiquantitative RT-PCR analysis of RRV-E2 gene expression (Fig. 2B and C). Using a reporter plasmid encoding luciferase under the control of the IFN-β promoter, RRV_{PERS}-infected cells also showed a 2-fold reduction in luciferase activity compared to that of RRV-T48-infected cells (Fig. 2D). ELISA analysis confirmed these observations, with 2.5-fold more IFN-β protein in cells infected with RRV-T48 than in cells infected with RRV_{PERS} (Fig. 2E). These observations clearly show that infection of RAW 264.7 cells with RRV_{PERS} induced less IFN-β than infection with RRV-T48 and suggest that the increased replication of RRV_{PERS} in RAW 264.7 cells (Fig. 1D) may due to lower levels of IFN-α/β induction.

In addition, we sought to exclude the possibility that reduced IFN-α/β production in cells infected with RRV_{PERS} was due to differences in the number of cells infected early during infection. The percentages of cells infected with each virus at 6, 12, and 24 h postinfection were measured. At 6 h postinfection, the percentages of cells infected with each virus were found to be similar (Fig. 2F). However, at 12 and 24 h postinfection, a higher percentage of RRV-positive cells was detected in cultures infected with RRV_{PERS} than in cultures infected with RRV-T48 (Fig. 2F). This result suggests that the differences in the induction of IFN-α/β between RRV-T48 and RRV_{PERS} were not due to differences in the percentage of cells infected at early time points after infection.

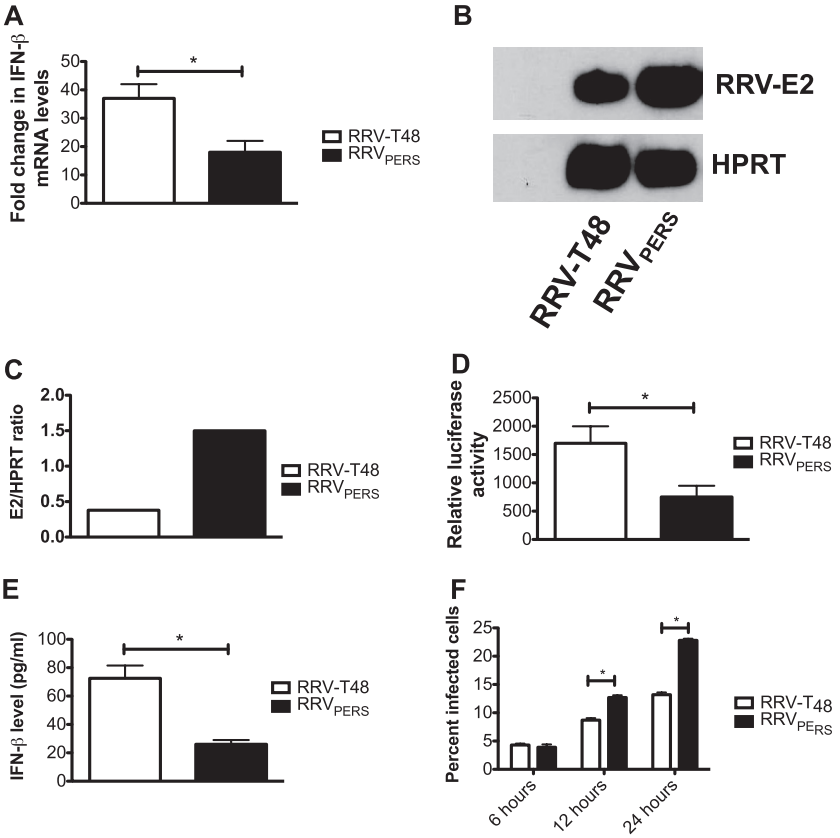

FIG. 2. RRV$_{PERS}$ infection of RAW 264.7 cells triggers lower IFN-β expression and production. (A) Quantitative real-time PCR analysis of transcript for IFN-β mRNA in RAW 264.7 cells 12 h after infection at an MOI of 0.1 with RRV-T48 or RRV$_{PERS}$. Data represent the mean fold change in mRNA levels from those for uninfected controls. GAPDH was used as a reference gene. Statistical analysis of relative expression results was performed using the REST software program. Significant differences in expression ($P < 0.05$) are marked with an asterisk. (B and C) Semiquantitative RT-PCR analysis of transcript for RRV E2 mRNA in RAW 264.7 cells 12 h after infection at an MOI of 0.1 with RRV-T48 or RRV$_{PERS}$. HPRT was used as a reference gene. Relative transcript levels were quantified in arbitrary units using the ImageJ software program (Image Processing and Analysis in Java; http://rsb.info.nih.gov/ij/). (D) Luciferase reporter gene activity at 12 h after infection of RAW 264.7 cells at an MOI of 0.1 with RRV-T48 or RRV$_{PERS}$. RAW264.7 cells were transiently transfected with the pIFN-β (−125/+72) Lucter reporter plasmid. Twenty-four hours later, cells were inoculated at an MOI of 0.1 with RRV-T48 or RRV$_{PERS}$, followed by cell lysis at 12 h postinfection. Luciferase activity was normalized to β-galactosidase reporter expression. Significant differences in expression ($P < 0.05$) are marked with an asterisk. (E) ELISA analysis of IFN-β protein production in RAW 264.7 cells 12 h after infection with 0.1 MOI of RRV-T48 or RRV$_{PERS}$. Significant differences in protein levels ($P < 0.05$) are marked with an asterisk. (F) Percentage of infected cells at 6, 12, and 24 h postinfection with 0.1 MOI RRV-T48 or RRV$_{PERS}$. Infected cells were detected using mouse anti-RRV hyperimmune ascitic fluid and fluorescein isothiocyanate (FITC)-conjugated sheep anti-mouse IgG antibody. Infected cells were counted using a Leica fluorescence microscope. Significant differences ($P < 0.05$) in cell numbers are indicated with an asterisk.

RRV$_{PERS}$ exhibits higher resistance to IFN-β-induced antiviral activity. We next investigated the effects of IFN-β treatment on the replication of RRV$_{PERS}$ and RRV-T48 in RAW 264.7 cells. RAW 264.7 cells were treated with 10, 50m or 100 IU IFN-β and infected 24 h later with RRV$_{PERS}$ or RRV-T48. The amount of virus in the cultures was determined by plaque assay, real-time PCR, and Western blotting. RRV$_{PERS}$ showed increased resistance to IFN-β-mediated antiviral activity, with RRV$_{PERS}$-infected cells generating a substantially higher viral load than cells infected with the parent RRV-T48 virus (Fig. 3A to D). Cells were also collected for Western blotting to analyze RRV E2 glycoprotein levels. Qualitative analysis reveal that at 24 h postinfection, RRV E2 levels were higher in RRV$_{PERS}$-infected cells than in those infected with RRV-T48 (Fig. 3E). These results indicate that RRV$_{PERS}$ has increased resistance to the antiviral activity of IFN-β.

Infection by RRV$_{PERS}$ shows inhibitory effects on type I IFN signaling. To determine whether the resistance of RRV$_{PERS}$ to IFN-β treatment is mediated by the inhibition of type I IFN signaling, a plasmid encoding the luciferase reporter gene under the control of type I IFN (ISRE)-responsive element was used. These studies were carried out with Vero cells, which are able to respond to IFN-α/β but do not produce these factors themselves. Induction of luciferase can thus be attributed exclusively to exogenously added IFN-β. Vero cells were transfected with the pISRE-luc plasmid, followed by infection with RRV-T48 or RRV$_{PERS}$ at an MOI of 5. IFN-β (100 IU/ml) was added 12 h later, and luciferase expression was measured 6 h later. Luciferase expression from the ISRE promoter in response to treatment with IFN-β was lower in cells infected with RRV$_{PERS}$ than in those infected with RRV-T48 (Fig. 4A), suggesting that RRV$_{PERS}$ is able to interfere with the IFN-α/β

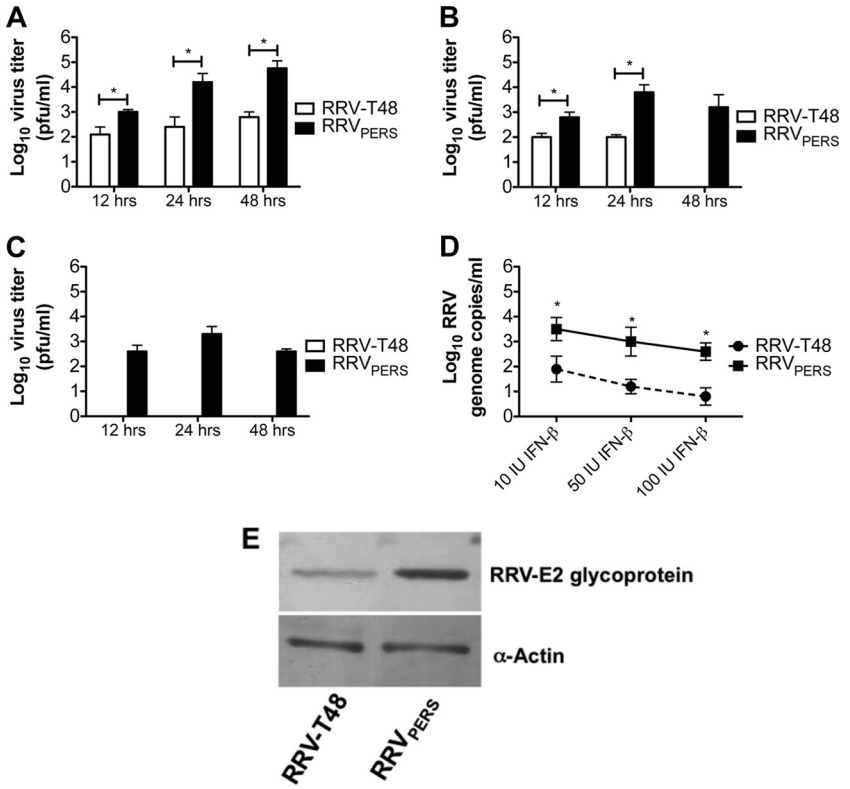

FIG. 3. RRV_{PERS} exhibits enhanced resistance to antiviral stimuli. Growth of RRV-T48 and RRV_{PERS} in RAW 264.7 cultures stimulated with 10 IU/ml (A), 50 IU/ml (B), or 100 IU/ml (C) IFN-β 24 h prior to RRV infection (MOI = 0.1). Culture supernatants were collected at 12, 24, and 48 h post-RRV infection, and viral growth was assessed by plaque assay on Vero cell monolayers. The assay limit of detection is 2.0 $\log_{10}$ PFU/ml. Significant differences in virus titers ($P < 0.05$) are marked with an asterisk. (D) Quantitation of the RRV genome by real-time PCR. RAW 264.7 cells were stimulated with 50 IU/ml IFN-β 24 h prior to RRV infection (MOI = 0.1). RNA was extracted at 24 h postinfection for the measurement of RRV genome copy numbers. Significant differences in viral genome copy numbers ($P < 0.05$) are indicated with an asterisk. (E) Total protein was obtained from RAW 264.7 cells stimulated with 50 IU/ml IFN-β 24 h prior to RRV infection (MOI = 0.1). Cell lysates were collected at 24 h postinfection for Western blot analysis using a polyclonal antibody against the RRV E2 glycoprotein. Detection of host cell protein expression by anti-α-actin was used to demonstrate equal loading of protein.

receptor signaling pathway to a greater extent than wild-type virus.

To further analyze IFN-α/β receptor signaling, we determined the levels of STAT-1 and STAT-2 phosphorylation in HEp-2 cells infected with RRV-T48 or RRV_{PERS} at an MOI of 5 for 12 h followed by IFN-β (100 IU/ml) treatment for 30 min. Treatment with IFN-β resulted in high levels of STAT-1 phosphorylation, but this was markedly reduced in cells infected with RRV_{PERS} from that in cells infected with RRV-T48 (Fig. 4B and *C*). There were no detectable differences in phosphorylated STAT-2, total STAT-1, total STAT-2, and α-actin in cells infected with either of the viruses (Fig. 4B and *C*). Similar results were obtained when the same experiment was performed with Vero cells (data not shown). Uninfected cells treated with IFN-β showed levels of phosphorylated STAT-1 and STAT-2 comparable to those for cells infected with RRV-T48 and treated with IFN-β (Fig. 4C). These results suggest that RRV_{PERS} and not RRV-T48 can interfere with the IFN-α/β receptor signaling pathway at the level of, or upstream of, STAT-1 phosphorylation. The observation that the inhibition of STAT-1 phosphorylation was not associated with detectable changes in STAT-2 phosphorylation, total STAT-1, total STAT-2, and α-actin levels suggests that shutdown of host protein synthesis was not responsible for this inhibition.

Infection of outbred mice with RRV_{PERS} results in enhanced mortality associated with high virus titers and reduced IFN-β. To determine whether the altered *in vitro* phenotype of RRV_{PERS} resulted in increased pathogenicity *in vivo*, we undertook infection studies in Swiss outbred mice, which have been used extensively in RRV pathogenesis studies (58, 59). Following infection of Swiss mice with a dose range of 10^4 to 10^6 PFU RRV (i.p.), markedly enhanced mortality was observed for mice infected with RRV_{PERS} compared to that for those infected with RRV-T48 (Fig. 5A, B, and C). Serum RRV titers were 1.5 $\log_{10}$ higher for RRV_{PERS}-infected mice than for RRV-T48-infected animals ($P < 0.05$) (Fig. 5D), suggesting that the increased mortality in mice infected with RRV_{PERS} was related to enhanced viral replication.

To determine whether RRV_{PERS} induces less IFN-β *in vivo*, lymph nodes from 5-week-old Swiss outbred mice at 1 day following infection with RRV-T48 or RRV_{PERS} were homogenized and analyzed for the presence of IFN-β by ELISA. Nearly 50% less IFN-β was detected in the lymph nodes of mice infected with RRV_{PERS} than in mice infected with the RRV-T48 (Fig. 5E).

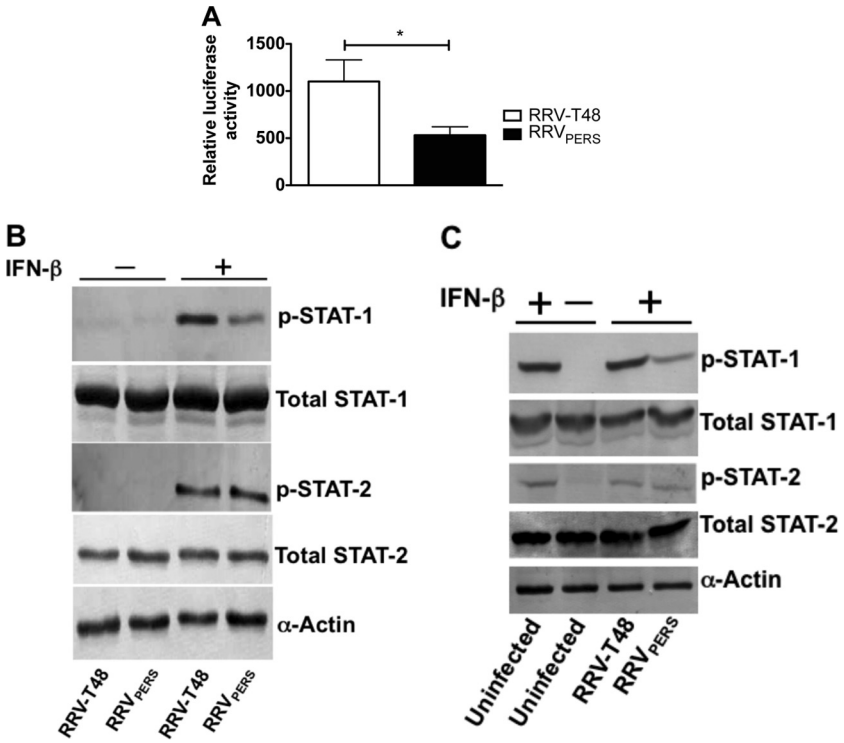

FIG. 4. Type I IFN signaling is inhibited in cells infected with RRV_{PERS}. (A) These studies were performed with Vero cells, which do not produce IFN but are able to respond to IFN. Vero cells were transfected with the pISRE (9-27) Lucter plasmid and then infected with RRV-T48 or RRV_{PERS} (5 MOI). IFN-β (100 IU/ml) was added 12 h later, and luciferase expression was measured following incubation for 6 h. Luciferase activity was normalized to β-galactosidase reporter expression. Significant differences in expression ($P < 0.05$) are marked with an asterisk. (B and C) Western blot analysis of STAT-1 and STAT-2 expression and phosphorylation in HEp2 cells infected with RRV-T48 or RRV_{PERS} (5 MOI) for 12 h, followed by IFN-β (100 IU/ml) treatment for 30 min or no treatment. The cell lysates were examined by Western blotting with antibodies to STAT-1, pY-STAT-1, STAT-2, or pY-STAT-2. The control included the detection of host cell protein expression by anti-α-actin antibody.

Infection of Swiss outbred mice with RRV_{PERS} results in enhanced severity of hind limb disease and myositis compared to results with parent virus. We recently demonstrated that Swiss outbred mice infected with RRV developed severe disease characterized by loss of hind limb gripping ability and altered gait. These disease signs correlated with inflammation of joint and skeletal muscle tissue (29, 38). Since RRV_{PERS} has enhanced virulence *in vivo* (Fig. 5), we examined its ability to induce arthritis and myositis in Swiss outbred mice. Eighteen-day-old mice were infected with 10^4 PFU RRV_{PERS} or RRV-T48, and mice were monitored for the development of disease signs. Infection of mice with RRV_{PERS} resulted in more-severe disease than infection with RRV-T48 (Fig. 6A). Mice infected with RRV_{PERS} reached a level of disease requiring euthanasia by day 10 postinfection.

To compare muscle tissue inflammation and pathology in mice infected with RRV_{PERS} and RRV-T48, histological analysis of skeletal muscle was performed. In RRV_{PERS}-infected mice, severe inflammation and tissue damage were observed in muscle tissue at 5 days postinfection (Fig. 6B, panels c and f). Inflammatory infiltrates were also observed in quadriceps skeletal muscle of RRV-T48-infected mice, but the level of inflammation was not as severe and tissue damage was not apparent at this time point (Fig. 6B, panels b and e).

DISCUSSION

In the present study, we characterized an RRV variant (RRV_{PERS}) that had been selected during persistent infection of a mouse macrophage cell line under antiviral conditions. RRV_{PERS} formed small plaques and possessed mutations in the structural and nsP regions. RRV_{PERS} induced lower levels of type I IFN and showed enhanced resistance to antiviral stimuli associated with inhibition of IFN-α/β signaling. In association with these changes, RRV_{PERS} was highly pathogenic, with increased disease severity and mortality following infection of mice.

Significant insights into the selection of an IFN-resistant viral phenotype have come through the study of human hepatitis C virus (HCV), which successfully persists in some patients (and cell cultures) for very long periods. The treatment of HCV patients with IFN is often stymied by the eventual development of IFN resistance by the virus. It has been suggested that exogenous IFN treatment could lead to selective pressure on the virus and the development of mutant strains able to resist IFN-mediated host defense (16, 27, 56). Sumpter et al. (56) found that persistent growth of HCV in cell culture was associated with genetic variation of viral NS5A, NS3, and NS4A, which endowed the virus with the ability to disrupt IFN regulatory factor 1 (IRF-1) and IRF-3 signaling following IFN

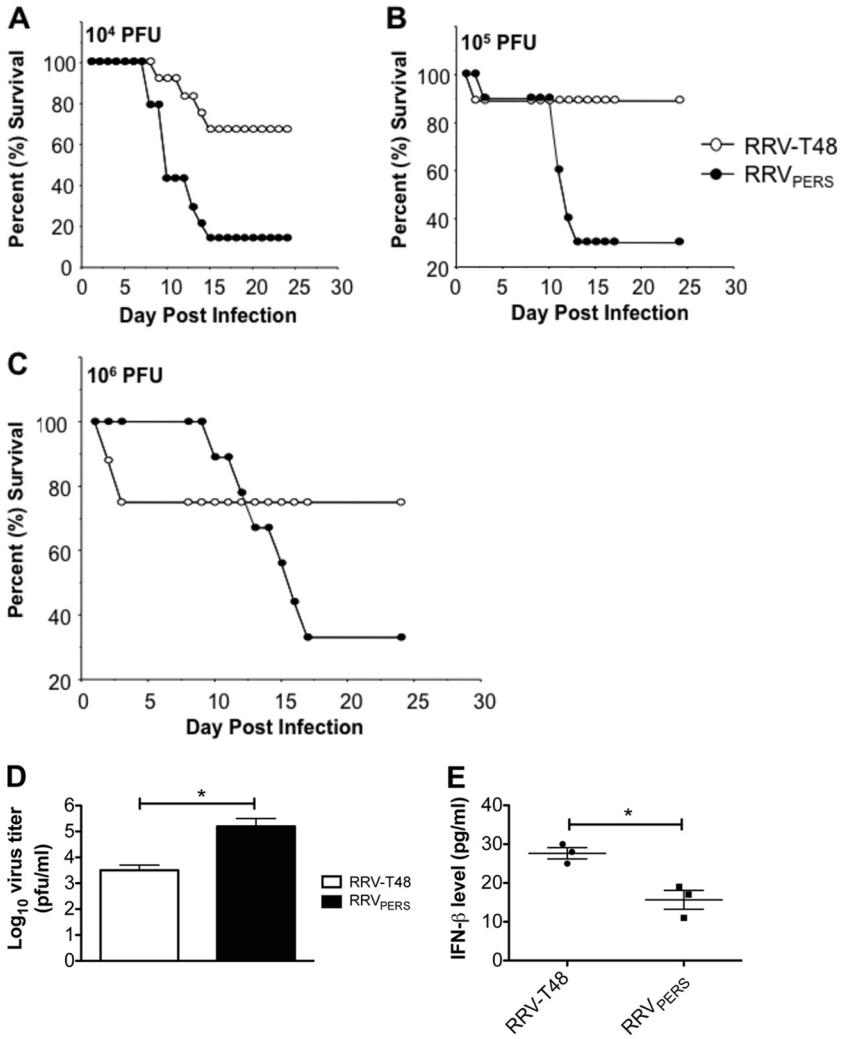

FIG. 5. RRV$_{PERS}$ infection in mice results in enhanced mortality associated with reduced IFN-β expression. (A to C) Survival of 14-day-old Swiss outbred mice after intraperitoneal (i.p.) infection with RRV-T48 (open circles) or RRV$_{PERS}$ (closed circles). Virus was inoculated at doses ranging from 10^4 (A) or 10^5 (B) to 10^6 (C) PFU/mouse ($n = 10$). Differences between survival curves were calculated using the log rank test. $P < 0.05$ was considered to be significant. (D) Titers of RRV-T48 and RRV$_{PERS}$ ($\log_{10}$ PFU/ml) in the serum of 14-day-old Swiss outbred mice infected subcutaneously (s.c.) 24 h previously with 10^4 PFU/mouse. The plaque assay limit of detection is 2.0 $\log_{10}$ PFU/ml. Significant differences in virus titers ($P < 0.05$) are marked with an asterisk. (E) IFN-β concentration in homogenized lymph nodes of 5-week-old Swiss outbred mice 24 h after s.c. infection with 10^4 PFU RRV-T48 or RRV$_{PERS}$ ($n = 3$ mice per group). Significant differences in protein levels ($P < 0.05$) are marked with an asterisk.

stimulation. HCV proteins have been linked to the attenuation of signaling via the IFN-α/β receptor (18), and HCV variant E2 and NS5A proteins have been demonstrated to bind PKR and interfere with IRF-1 stimulation (41, 57). The ability of HCV to modulate the activity of type 1 IFN may contribute to its ability to persist in the host. In the present study, we observed that small-plaque variants also arose in unstimulated RAW 264.7 cells but at a much lower rate than in cultures stimulated with LPS. This observation is consistent with the model that has been proposed for HCV infection (56), in which exogenous IFN can drive the evolution of strains resistant to IFN-mediated antiviral activity.

Alphaviruses efficiently induce IFN-α/β and are also generally highly sensitive to the antiviral effects of IFN-α/β (3, 46, 62). For instance, based on human and mouse studies, low levels of IFN-β can efficiently inhibit chikungunya virus (CHIKV) infection (46). Mice deficient in the IFN-α/β receptor (IFN-α/β $R^{-/-}$) are highly susceptible to CHIKV infection, with infection resulting in death within 3 days (8). Similarly, RRV infection resulted in substantial mortality in IFN-α receptor-deficient mice (IFN-α $R^{-/-}$), while wild-type mice were able to resist infection (J. Podger and S. Mahalingam, unpublished data). In terms of induction and sensitivity to IFN, our results show that RRV$_{PERS}$ induces less IFN-β and exhibits resistance to its antiviral effects compared to the parent virus.

Mortality and disease severity were greatly enhanced in mice infected with RRV$_{PERS}$ compared to those infected with RRV-T48. The reduction in IFN-β production observed *in vitro* following infection with RRV$_{PERS}$ was also observed *in vivo*, with a 50% reduction in IFN-β levels in the lymph nodes of mice infected with RRV$_{PERS}$ compared to results for those infected with RRV-T48. It is likely that the virus-mediated

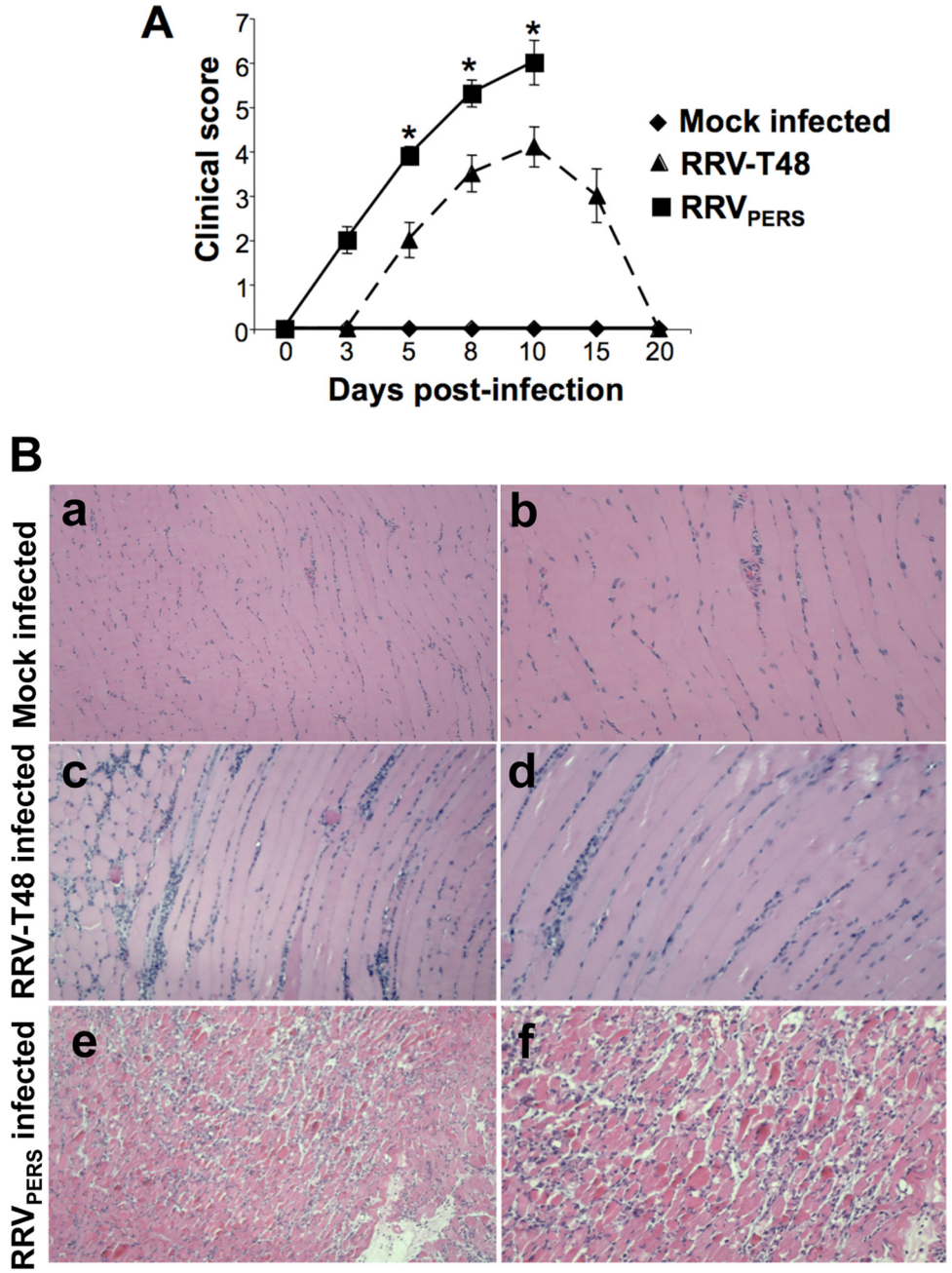

FIG. 6. RRV$_{PERS}$ induced severe RRVD in a mouse model of disease. Eighteen-day-old outbred mice were infected with 10^4 PFU of RRV-T48 or RRV$_{PERS}$ by injection in the left rear footpad. (A) Mice were scored for development of hind limb dysfunction and disease based on the following scale: 0, no disease; 1, ruffled fur; 2, very mild hind limb weakness; 3, mild hind limb weakness; 4, moderate hind limb weakness; 5, severe hind limb weakness/dragging; 6, complete loss of hind limb function; 7, moribund; 8, dead ($n = 5$). Data for disease scores were analyzed by the Mann-Whitney test. Significant differences in disease score ($P < 0.05$) are indicated with an asterisk. (B) Eighteen-day-old outbred mice were infected with 10^4 PFU of RRV by injection in the left rear footpad. At 5 days p.i., mice were perfused with 4% paraformaldehyde, and 5-μm-thick paraffin-embedded sections generated from quadriceps muscle were hematoxylin and eosin (H&E) stained; (a) Mock; (b) RRV-T48-infected mice; (c) RRV$_{PERS}$-infected mice. Images are representative of at least 3 mice per group. Magnifications: a, c, and e, ×100; b, d, and f, ×200.

inhibition of the type I IFN response contributes to disease exacerbation following infection with RRV$_{PERS}$. Our results are reminiscent of findings with Venezuelan equine encephalitis virus (VEEV), in which infection of mice with an IFN-resistant strain resulted in enhanced clinical disease (51). Similar results were obtained with an IFN-α/β-resistant eastern equine encephalitis virus (EEEV) strain; infection of mice with this strain resulted in enhanced encephalitis, an effect that mapped to both structural and nonstructural genes (1).

To counteract type I IFN responses, many viruses encode proteins that disrupt type I IFN signaling and downstream responses. These evasion strategies have been linked to viral

pathogenesis and the emergence of virus in new host populations (24, 51). Suppression of type I IFN responses has been observed for influenza virus (4, 14), dengue virus (20, 39), West Nile virus (32) and other RNA viruses (reviewed in references 15 and 35). Many viral proteins have been reported to block transcription factors that control production of type I IFN (reviewed in references 14, 15, and 35). In this study we have identified RRV as an additional member capable of developing mechanisms to suppress IFN responses. Alphavirus infection results in rapid shutdown of host cell protein synthesis in favor of viral protein synthesis, and the conventional view has been that this mechanism underlies the observed suppression of IFN-α/β production (44). For example, the nsP2 proteins of Sindbis virus and Semliki Forest virus (SFV) can inhibit type I IFN responses via host protein shutdown (5, 12), while the capsid proteins of EEEV and VEEV perform a similar IFN-targeting function (1, 2, 51). Mutating the nuclear localization sequence of nsP2 of SFV resulted in a virus that induced more IFN-α/β, suggesting that nsP2 inhibits IFN-α/β induction (5). However, those authors admit that an alternative explanation is that relocalization of nsP2 may simply result in more-effective induction of IFN-α/β (5). Alphaviruses might also exert much more specific effects on the IFN-α/β system independent of host protein shutoff. Our earlier studies with RRV demonstrated that Fc receptor bearing cells (dendritic cells [DCs] and macrophages) can be infected via a mechanism involving antibody-dependent enhancement (ADE) of infection and that this results in interleukin 10 (IL-10)-dependent inhibition of cellular IFN-α/β production (34). We have also demonstrated that the presence of high-mannose glycans on virus derived from mosquito cells interferes with type I IFN induction in myeloid DCs (47). Recently, Yin and colleagues reported that the phosphorylation of STAT-1 and STAT-2 was partially blocked by VEEV and Sindbis virus and the effect was dependent on the expression of viral nsP (61). In another study, Simmons et al. showed that VEEV can antagonize STAT-1 activation following type I IFN treatment and that the inhibition of type I IFN signaling occurred via distinct mechanisms independent of host protein shutoff (49). Cruz et al. have identified a mutation in the nsP1/nsP2 cleavage domains of Sindbis virus and RRV associated with a specific enhancement of IFN production independent of virus-induced host shutoff (9). More recently, Fros et al. showed that chikungunya virus infection blocked IFN-induced STAT-1 phosphorylation and that this inhibition was mediated by nsP2 and was independent of host shutoff (13). Several lines of evidence also suggest that shutdown of host protein synthesis is not responsible for the RRV_{PERS}-mediated IFN-α/β signaling inhibition. First, the reduced levels of phosphorylated STAT-1 were not associated with reduced total STAT-1 levels, which suggests that the inhibition was not due to decreased synthesis of total STAT-1. Second, phosphorylated STAT-2, total STAT-2, and housekeeping gene α-actin levels were not decreased by RRV_{PERS} infection, which indicates that the small-plaque variant specifically targets STAT-1. Third, the STAT-1 and STAT-2 levels in uninfected controls treated with IFN were comparable to levels in cells infected with RRV-T48 and treated with IFN, suggesting that RRV-T48 does not inhibit phosphorylation of STAT-1 or -2 and that the effects are specific to RRV_{PERS}.

The ability of viruses to develop resistance to host antiviral activity by genetic sequence variation has a major effect on virus virulence and persistence in the host. Mutational studies have shown that alphaviruses appear to attain these effects mainly through the action of nsPs (1, 2, 5, 9, 13, 51). We identified a number of mutations in nsP1 to *nsP*4 and a single mutation in E2 in RRV_{PERS}. Using site-directed mutagenesis, we introduced the RRV_{PERS} E2 mutation into the parent RRV-T48 cDNA infectious clone (adenine to uracil [GAG→GUG] at position E2-347). Interestingly, the mutation in E2 did not affect IFN induction and resistance of RRV_{PERS} (data not shown). Future studies will investigate whether these mutations in the nsP regions are involved in the perturbation of IFN signaling pathways that we observed. Our preliminary studies (using chimeric virus and a pcDNA plasmid expressing nonstructural genes) show that RRV_{PERS} nsP1 and nsP2 are able to inhibit IFN-α/β signaling (data not shown), and we are currently attempting to identify the mechanisms of action. Future studies will introduce the mutations that we identified in the RRV_{PERS} nsPs into the wild-type RRV infectious clone (pRR64), followed by testing of the IFN resistance phenotype and pathogenicity of the recombinant virus. If the IFN resistance phenotype of RRV_{PERS} is recovered, examination of the expression of downstream IFN-induced proteins will be investigated. These studies will allow us to identify the specific nsP mutation(s) that leads to the IFN suppression phenotype induced by enhanced macrophage inflammatory activity.

In conclusion, we describe *in vitro* and *in vivo* studies characterizing the genetic and phenotypic properties of a novel small-plaque, persistent strain of RRV. The enhanced suppression of IFN signaling mediated by RRV_{PERS} is likely to play a key role in the enhanced pathogenicity exhibited by this virus. This study demonstrates that selective pressure exerted by host antiviral activity can promote the evolution of an IFN-resistant, persistent, and highly pathogenic alphavirus strain. It is possible that a similar evolutionary mechanism may operate *in vivo*, and sequencing of clinical isolates from persistent alphavirus infections will provide new insights into viral pathogenesis in human disease.

ACKNOWLEDGMENTS

This work is supported by an Australian National Health and Medical Research Council (NHMRC) grant (no. 399700). S.M. is the recipient of the Australian Research Council Future Fellowship. M.S.R. and A.S. are recipients of the Australian NHMRC RD Wright Fellowship and Principal Research Fellowship, respectively.

We thank Kalani Ruberu and Sancho Bartels for their early help with the small-plaque studies. We also thank Roy Hall (University of Queensland [Australia]) and Mark Heise (University of North Carolina) for critical reading of the manuscript and useful discussions.

REFERENCES

1. **Aguilar, P. V., S. C. Weaver, and C. F. Basler.** 2007. Capsid protein of eastern equine encephalitis virus inhibits host cell gene expression. J. Virol. **81:**3866–3876.
2. **Aguilar, P. V., et al.** 2008. Structural and nonstructural protein genome regions of eastern equine encephalitis virus are determinants of interferon sensitivity and murine virulence. J. Virol. **82:**4920–4930.
3. **Antalis, T. M., et al.** 2008. The serine proteinase inhibitor (serpin) plasminogen activation inhibitor type 2 protects against viral cytopathic effects by constitutive interferon alpha/beta priming J. Exp. Med. **187:**1799–1811.
4. **Bergmann, M., et al.** 2000. Influenza virus NS1 protein counteracts PKR-mediated inhibition of replication. J. Virol. **74:**6203–6206.
5. **Breakwell, L., et al.** 2007. Semliki Forest virus nonstructural protein 2 is involved in suppression of the type I interferon response. J. Virol. **81:**8677–8684.
6. **Broom, A. K., et al.** 1998. Identification of Australian arboviruses in inoculated cell cultures using monoclonal antibodies in ELISA. Pathology **30:**286–288.

7. **Chomczynski, P., and N. Sacchi.** 1987. Single-step method of RNA isolation by acid guanidinium thiocyanate-phenol-chloroform extraction. Anal. Biochem. **162:**156–159.
8. **Couderc, T., et al.** 2008. A mouse model for Chikungunya: young age and inefficient type-I interferon signaling are risk factors for severe disease. PLoS Pathog. **4**(2)**:**e29.
9. **Cruz, C. C., et al.** 2010. Modulation of type I IFN induction by a virulence determinant within the alphavirus nsP1 protein. Virology **399:**1–10.
10. **Faragher, S. G., A. D. J. Meek, C. M. Rice, and L. Dalgarno.** 1988. Genome sequences of a mouse-avirulent and a mouse-virulent strain of Ross River virus. Virology **163:**509–526.
11. **Friedman, R. M., and J. M. Ramseur.** 1979. Mechanisms of persistent infections by cytopathic viruses in tissue culture. Arch. Virol. **60:**83–103.
12. **Frolova, E. I., et al.** 2002. Roles of non-structural protein nsP2 and alpha/beta interferons in determining the outcome of Sindbis virus infection. J. Virol. **76:**11254–11264.
13. **Fros, J. J., et al.** 2010. Chikungunya virus nonstructural protein 2 inhibits type I/II interferon-stimulated JAK-STAT signaling. J. Virol. **84:**10877–10887.
14. **Garcia-Sastre, A.** 2001. Inhibition of interferon-mediated antiviral responses by influenza A viruses and other negative-strand RNA viruses. Virology **279:**375–384.
15. **Garcia-Sastre, A.** 2004. Identification and characterization of viral antagonists of type I interferon in negative-strand RNA viruses. Curr. Top. Microbiol. Immunol. **283:**249–280.
16. **Hanada, K., Y. Tanaka, M. Mizokami, T. Gojobori, and H. J. Alter.** 2007. A reduction in selective immune pressure during the course of chronic hepatitis C correlates with diminished biochemical evidence of hepatic inflammation. Virology **361:**27–33.
17. **Harley, D., A. Sleigh, and A. Ritchie.** 2001. Ross River virus transmission, infection, and disease: a cross-disciplinary review. Clin. Microbiol. Rev. **14:**909–932.
18. **Heim, M. H., D. Moradpour, and H. E. Blum.** 1999. Expression of hepatitis C virus proteins inhibits signal transduction through the Jak-STAT pathway. J. Virol. **73:**8469–8475.
19. **Hoarau, J. J., et al.** 2010. Persistent chronic inflammation and infection by Chikungunya arthritogenic alphavirus in spite of a robust host immune response. J. Immunol. **184:**5914–5927.
20. **Jones, M., et al.** 2005. Dengue virus inhibits alpha interferon signaling by reducing STAT2 expression. J. Virol. **79:**5414–5420.
21. **Journeaux, S. F., W. G. Brown, and J. G. Aaskov.** 1987. Prolonged infection of human synovial cells with Ross River virus. J. Gen. Virol. **68:**3165–3169.
22. **Josseran, L., et al.** 2006. Chikungunya disease outbreak, Reunion Island. Emerg. Infect. Dis. **12:**1994–1995.
23. **Kalantri, S. P., R. Joshi, and L. W. Riley.** 2006. Chikungunya epidemic: an Indian perspective. Natl. Med. J. India **19:**315–322.
24. **Keller, B. C., et al.** 2006. Resistance to alpha/beta interferon is a determinant of West Nile virus replication fitness and virulence. J. Virol. **80:**9424–9434.
25. **Kuhn, R. J., H. G. Niesters, Z. Hong, and J. H. Strauss.** 1991. Infectious RNA transcripts from Ross River virus cDNA clones and the construction and characterization of defined chimeras with Sindbis virus. Virology **182:**430–441.
26. **Labadie, K., et al.** 2010. Chikungunya disease in nonhuman primates involves long-term viral persistence in macrophages. J. Clin. Invest. **120:**894–906.
27. **Lidbury, B. A.** 1994. Was exposure to directly antiviral cytokines during primary infection an important selective pressure in the evolution of unique immune evasion strategies by viruses? Immunol. Cell Biol. **72:**347–350.
28. **Lidbury, B. A., C. Simeonovic, G. E. Maxwell, I. D. Marshall, and A. J. Hapel.** 2000. Macrophage-induced muscle pathology results in morbidity and mortality for Ross River virus infected mice. J. Infect. Dis. **181:**27–34.
29. **Lidbury, B. A., et al.** 2008. Macrophage-derived pro-inflammatory factors contribute to the development of arthritis and myositis following infection with an arthrogenic alphavirus. J. Infect. Dis. **197:**1585–1593.
30. **Lidbury, B. A., and S. Mahalingam.** 2000. Specific ablation of antiviral gene expression in macrophages by antibody dependent enhancement of Ross River virus infection. J. Virol. **74:**8376–8381.
31. **Linn, M. L., J. G. Aaskov, and A. Suhrbier.** 1996. Antibody-dependent enhancement and persistence in macrophages of an arbovirus associated with arthritis. J. Gen. Virol. **77:**407–411.
32. **Liu, W. J., et al.** 2005. Inhibition of interferon signaling by the New York 99 strain and Kunjin subtype of West Nile virus involves blockage of STAT1 and STAT2 activation by nonstructural proteins. J. Virol. **79:**1934–1942.
33. **Luers, A. J., S. D. Adams, J. V. Smalley, and J. J. Campanella.** 2005. A phylogenomic study of the genus alphavirus employing whole genome comparison. Comp. Funct. Genomics **6:**217–227.
34. **Mahalingam, S., and B. A. Lidbury.** 2002. Suppression of lipopolysaccharide-induced antiviral transcription factor (STAT1 and NF-kappa B) complexes by antibody-dependent enhancement of macrophage infection by Ross River virus. Proc. Natl. Acad. Sci. U. S. A. **99:**13819–13824.
35. **Mahalingam, S., J. Meanger, P. S. Foster, and B. A. Lidbury.** 2002. The viral manipulation of the host cellular and immune environments to enhance propagation and survival: a focus on RNA viruses. J. Leukoc. Biol. **72:**429–439.
36. **Mateo, L., et al.** 2000. An arthrogenic alphavirus induces monocyte chemoattractant protein 1 and interleukin-8. Intervirology **43:**55–60.
37. **Mavalankar, D., P. Shastri, T. Bandyopadhyay, J. Parmar, and K. V. Ramani.** 2008. Increased mortality rate associated with Chikungunya epidemic, Ahmedabad, India. Emerg. Infect. Dis. **14:**412–415.
38. **Morrison, T. E., et al.** 2006. Characterization of Ross River virus tropism and virus-induced inflammation in a mouse model of viral arthritis and myositis. J. Virol. **80:**737–749.
39. **Munoz-Jordan, J. L., G. G. Sanchez-Burgos, M. Laurent-Rolle, and A. Garcia-Sastre.** 2003. Inhibition of interferon signaling by dengue virus. Proc. Natl. Acad. Sci. U. S. A. **100:**14333–14338.
40. **Mylonas, A. D., et al.** 2002. Natural history of Ross River virus-induced epidemic polyarthritis. Med. J. Aust. **177:**356–360.
41. **Podevin, P., et al.** 2001. Expression of hepatitis C virus NS5A natural mutants in a hepatocytic cell line inhibits the antiviral effect of interferon in a PKR-independent manner. Hepatology **33:**1503–1511.
42. **Rulli, N. E., et al.** 2005. Ross River virus: molecular and cellular aspects of disease pathogenesis. Pharmacol. Ther. **107:**329–342.
43. **Rulli, N. E., et al.** 2009. Bindarit, an inhibitor of monocyte chemotactic proteins (MCPs) subfamily of CC chemokines, ameliorates alphavirus-induced arthritis and myositis in a mouse model. Arthritis Rheum. **60:**2513–2523.
44. **Ryman, K. D., and W. B. Klimstra.** 2008. Host responses to alphavirus infection. Immunol. Rev. **225:**27–45.
45. **Scharf, S. J., G. T. Horn, and H. A. Erlich.** 1986. Direct cloning and sequence analysis of enzymatically amplified genomic sequences. Science **233:**1076–1078.
46. **Schilte, C., et al.** 2010. Type I IFN controls Chikungunya virus via its action on nonhematopoietic cells. J. Exp. Med. **207:**429–442.
47. **Shabman, R. S., et al.** 2007. Differential induction of type I interferon responses in myeloid dendritic cells by mosquito and mammalian-cell-derived alphaviruses. J. Virol. **81:**237–247.
48. **Shabman, R. S., K. M. Rogers, and M. T. Heise.** 2008. Ross River virus envelope glycans contribute to type I interferon production in myeloid dendritic cells. J. Virol. **82:**12374–12383.
49. **Simmons, J. D., et al.** 2009. Venezuelan equine encephalitis virus disrupts Stat-1 signaling by distinct mechanisms independent of host shutoff. J. Virol. **83:**10571–10581.
50. **Soden, M., et al.** 2000. Detection of viral ribonucleic acid and histologic analysis of inflamed synovium in Ross River virus infection. Arthritis Rheum. **43:**365–369.
51. **Spotts, D. R., R. M. Reich, M. A. Kalkhan, R. M. Kinney, and J. T. Roehrig.** 1998. Resistance to alpha/beta interferons correlates with the epizootic and virulence potential of Venezuelan equine encephalitis viruses and is determined by the 5′ noncoding region and glycoproteins. J. Virol. **72:**10286–10291.
52. **Srivastava, U., M. Nelson, Y. C. Su, and S. Mahalingam.** 2008. Mechanisms of Chikungunya virus disease informed by Ross River virus research. Future Virol. **3:**509–511.
53. **Strauss, J. H., and E. G. Strauss.** 1994. The alphaviruses: gene expression, replication, and evolution. Microbiol. Rev. **58:**491–562.
54. **Suhrbier, A., and M. L. Linn.** 2004. Clinical and pathologic aspects of arthritis due to Ross River virus and other alphaviruses. Curr. Opin. Rheumatol. **16:**374–379.
55. **Suhrbier, A., and S. Mahalingam.** 2009. The immunobiology of viral arthritides. Pharmacol. Ther. **124:**301–308.
56. **Sumpter, R. Jr., C. Wang, E. Foy, Y. M. Loo, and M. Gale, Jr.** 2004. Viral evolution and interferon resistance of hepatitis C virus RNA replication in a cell culture model. J. Virol. **78:**11591–11604.
57. **Taylor, D. R., S. T. Shi, P. R. Romano, G. N. Barber, and M. M. Lai.** 1999. Inhibition of the interferon-inducible protein kinase PKR by HCV E2 protein. Science **285:**107–110.
58. **Vrati, S., P. J. Kerr, R. C. Weir, and L. Dalgarno.** 1996. Entry kinetics and mouse virulence of Ross River virus mutants altered in neutralization epitopes. J. Virol. **70:**1745–1750.
59. **Vrati, S., S. G. Faragher, R. C. Weir, and L. Dalgarno.** 1986. Ross River virus mutant with a deletion in the E2 gene: properties of the virion, virus-specific macromolecule synthesis, and attenuation of virulence for mice. Virology **151:**222–232.
60. **Way, S. J., B. A. Lidbury, and J. L. Banyer.** 2002. Persistent Ross River virus infection of murine macrophages: an in vitro model for the study of viral relapse and immune modulation during long-term infection. Virology **301:**281–292.
61. **Yin, J., C. L. Gardner, C. W. Burke, K. D. Ryman, and W. B. Klimstra.** 2009. Similarities and differences in antagonism of the neuron alpha/beta interferon response by Venezuelan equine encephalitis and Sindbis alphaviruses. J. Virol. **83:**10036–10047.
62. **Zhang, Y., C. W. Burke, K. D. Ryman, and W. B. Klimstra.** 2007. Identification and characterization of interferon-induced proteins that inhibit alphavirus replication. J. Virol. **81:**11246–11255.